第36卷第5期 红外与毫米波学报 Vol. 36, No.5
2017年10月 J. Infrared Millim. Waves October,2017

文章编号: 1001-9014(2017)05-0550-05 DOI:10.11972/j.issn.1001-9014.2017.05.007

Radio-Frequency modeling and parameters extraction of multi-cell MOSFET device

ZHOU Ying, YU Pan-Pan, GAO Jian-Jun*

(School of Information Science and Technology, East China Normal University, Shanghai 200062, China)

Abstract: An improved small-signal model for nanometer metal-oxide-semiconductor field-effect transistor (MOSFET) device is presented in this paper. The skin effect and multiple-cell effect are both taken into account. In the extracting procedure, the parameters of elementary cells are determined from the conventional model based on the scalable rules. This small-signal model was validated by the good agreement between measured and simulated S-parameters of 8×0.6×12 μm (number of gate fingers × unit gatewidth × cells) 90-nm gatelength MOSFET under three bias points up to 40 GHz.

Key words: semi-conductor technology, small-signal model, parameter extraction of model, skin effect, multi-cell model

PACS: 85.30.De

多胞 MOSFET 器件的射频建模和参数提取

周 影, 于盼盼, 高建军*

(华东师范大学 信息科学技术学院 电子工程系,上海 200062)

摘要:对纳米级金属氧化物半导体场效应管器件提出了改进的小信号模型.该改进模型中综合考虑了馈线的趋肤效应和器件多胞结构的影响.提取过程中,根据可缩放规律,由传统模型的参数推导出元胞参数.将模型应用于8×0.6×12 μm(栅指数×栅宽×元胞数量)、栅长为90 nm的MOSFET器件在1~40 GHz范围内的建模,测试所得S参数和模型仿真所得S参数能够高度地吻合.

关 键 词:半导体技术;小信号模型;模型参数提取;趋肤效应;多胞模型

中图分类号:TN386.1 **文献标识码**:A

Introduction

Radio frequency integrated circuits (RFIC) based on CMOS processes are currently receiving a significant amount of attention for the low cost and low-power characteristics of CMOS technology relative to other technologies. Downscaling of minimum transistor channel length makes the devices usable to frequencies in the gigahertz range. The performance of integrated devices is updated at a very fast pace. It is critical that these models are updated at a similar pace[1]. Designing RF circuits requires accurate models to describe the RF behavior of the devices.

Conventional models are based on device structures, which are made up of only one elementary cell. Those models are not suitable for multiple-cell devices, and the behavior of these devices cannot be predicted correctly. A more reliable model is necessary to characterize such multiple-cell devices.

The improved model adopting multiple cells to describe the RF performance of the large-size devices is verified by 90-nm MOSFET devices fabricated by Infineon Technologies, Munich, Germany. The measurement was performed at frequency range of 1~40 GHz at three biases. In comparison with previous publications, this model has following improvements:

1) The skin effect of feedlines is taken into account.

2) The effect of connections between elementary

Received date: 2017-04-17, **revised date**: 2017-06-27 **收稿日期**:2017-04-17, **修回日期**:2017-06-27

Foundation items: Supported by the National Natural Science Foundation of China (61474044)

Biography: ZHOU Ying (1993-), female, Shanghai, China. master. Research area involves microwave device modeling. E-mail: 18801965859@163.com

* **Corresponding author**: E-mail: jjgao@ee.ecnu.edu.cn

cells is supplemented into this model.

Therefore the model is more suitable for large-size devices consisting of multiple cells.

This paper is organized as follows. The equivalent circuit model of small-signal and the basic theory of extracting parameters of MOSFET are presented in Sect. 1. The extracting procedure is demonstrated in Sect. 2. In Sect. 3, experimental validation of the proposed method is described. The conclusions are presented in Sect. 4.

1 Theoretical analysis

1.1 Conventional Equivalent Circuit Model

The cubic diagram of conventional small-signal equivalent circuit model of MOSFET demonstrating the physical meanings of the parameters is shown in Fig. 1. The parasitics of the pad are modeled by the capacitances C_{pd} and C_{pg} in series with the resistances R_{pd} and R_{pg}. The resistance R_g represents the effective gate resistance that consists of the distributed channel resistance and the gate electrode resistance. The source and drain resistances, R_s and R_d are dominated by the resistance of the lightly doped extensions of the source and drain diffusions. C_{gs}, C_{gd} and C_{ds} represent the overlap capacitances merged with the correspondent intrinsic capacitances. $C_{gs} = C'_{gs} + C''_{gs}$, is consisting of the gate-channel capacitance C''_{gs} and the capacitance of the gate-source overlap C'_{gs}, C_{gd} is mainly due to the gate-drain overlap, and C_{ds} is the drain-to-source capacitance. g_m is the transconductance, R_{ds} is the drain resistance and τ is the time delay associated with the transconductance. MOSFET is fabricated on a resistive substrate, the substrate coupling between the drain and the bulk terminals is represented by the series connection of the substrate resistance R_{sub} and the drain junction capacitance C_{jd}. For applications of high-frequencies, the source is always tied to the substrate. It is also noted that the gate to bulk capacitance is incorporated into the intrinsic gate-to-source capacitance C_{gs}.

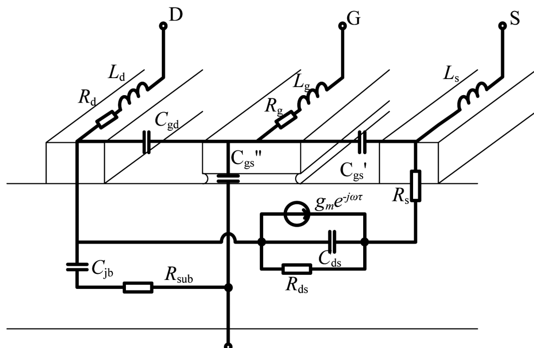

Fig. 1 Cubic diagram of conventional equivalent circuit model of MOSFET

图 1 MOSFET 传统等效电路模型的立体图

1.2 Proposed Equivalent Circuit Model

Figure 2 shows the proposed cubic equivalent circuit model of the test structure. It is better to take the skin effect of the feedline into account. R_{lga}, R_{lda} and R_{lsa} are the losses of the feedlines, L_{lga}, L_{lda} and L_{lsa} are the corresponding inductances. Three pairs of parallel inductances and resistances R_{lgb}, L_{lgb}, R_{ldb}, L_{ldb}, R_{lsb} and L_{lsb} model both the drop of inductances and the increase of line resistances due to the skin-effect in the feedlines.

Figure 3 shows the schematic layout of large-size MOSFET, which consists of multiple elementary cells. The proposed equivalent circuit model is illustrated in Fig. 4. The details inside the elementary cell are shown in Fig. 5. The principal improvement over the conventional model is that the proposed model considers both the skin effect of feedlines and multiple-cell effect. Large-size MOSFET actually consists of more than one cell, multiple cells help to increase the currents flowing from gate to source and from drain to source, then the gain of the multiplier using the MOSFET is improved. L_g^e, L_d^e and L_s^e represent the effect of the interconnections between the elementary cells.

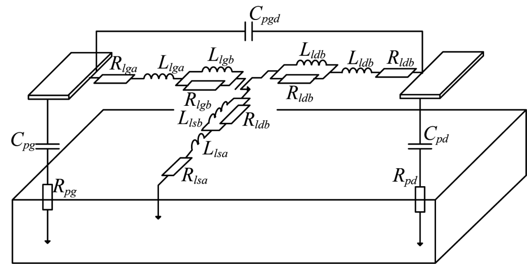

Fig. 2 Cubic diagram of the proposed equivalent circuit model of the test structure

图 2 提出的测试结构模型立体图

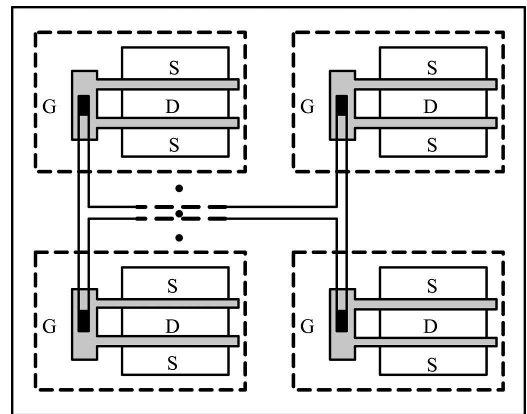

Fig. 3 Schematic layout of MOSFET which consists of multiple elementary cells

图 3 多胞 MOSFET 器件的电路版图

2 Parameters extraction technique

2.1 Parameter Extraction of Test Structure

The parasitic elements of pad C_{pd}, C_{pg}, C_{pgd}, R_{pd} and R_{pg} are extracted through the measured S-parameters of the open structure, R_{lga}, R_{lgb}, L_{lga}, L_{lgb}, R_{lda}, R_{ldb}, L_{lda}, L_{ldb}, R_{lsa}, R_{lsb}, L_{lsa} and L_{lsb} can be extracted from the Z-parameters of the measured short test structure u-

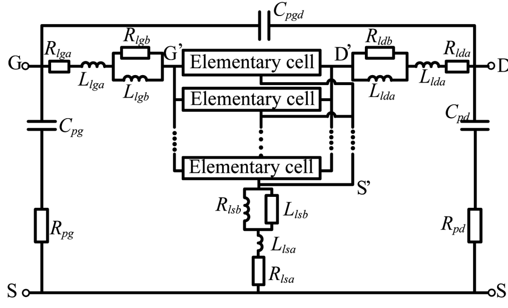

Fig. 4 Proposed model consisting of multiple cells
图 4 提出的多胞器件结构的电路模型

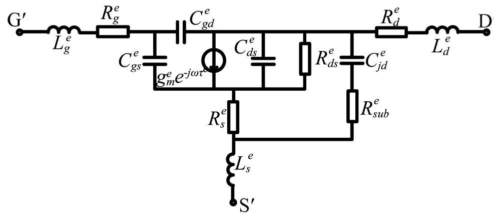

Fig. 5 Small-signal model for elementary cell
图 5 元胞内部的小信号模型

sing the following equations:

$$Z_{ld} = R_{lda} + j\omega L_{lda} + j\omega R_{ldb} L_{ldb} / (j\omega L_{ldb} + R_{ldb}) \quad , \quad (1)$$

$$Z_{ld} = R_{lda} + j\omega L_{lda} + j\omega R_{ldb} L_{ldb} / (j\omega L_{ldb} + R_{ldb}) \quad , \quad (2)$$

$$Z_{ls} = R_{lsa} + j\omega L_{lsa} + j\omega R_{lsb} L_{lsb} / (j\omega L_{lsb} + R_{lsb}) \quad , \quad (3)$$

where Z_{lg}, Z_{ld} and Z_{ls} represent the impedance of the feedline connecting the gate to the pad, the feedline connecting the drain to the pad, and the feedline connecting the source to the pad, respectively.

2.2 Parameters extraction of proposed small-signal model with multiple cells

Step 1

First, the multiple cells are regarded as the one cell in the conventional way. The Z-parameters of the one cell $Z_{pq}^{\mathrm{MOS}}(p, q = 1, 2)$ can be extracted by de-embedding pad and feedline parasitics. Then setting the initial values of R_g, R_d, R_s, C_{jd} and R_{sub}, the Z-parameters of the intrinsic part Z_{pq}^{INT} can be obtained by subtracting the parasitic effects associated with R_g, R_d, R_s, C_{jd} and R_{sub} using Eqs. 4-9:

$$Z_{11}^{\mathrm{MOS}} = (Z_{11}^{\mathrm{INT}} + R_s + Y_{jd} N) / [1 + (Z_{22}^{\mathrm{INT}} + R_s) Y_{jd}] + R_g \quad , \quad (4)$$

$$Z_{12}^{\mathrm{MOS}} = (Z_{12}^{\mathrm{INT}} + R_s) / [1 + (Z_{22}^{\mathrm{INT}} + R_s) Y_{jd}] \quad , \quad (5)$$

$$Z_{21}^{\mathrm{MOS}} = (Z_{21}^{\mathrm{INT}} + R_s) / [1 + (Z_{22}^{\mathrm{INT}} + R_s) Y_{jd}] \quad , \quad (6)$$

$$Z_{22}^{\mathrm{MOS}} = (Z_{22}^{\mathrm{INT}} + R_s) / [1 + (Z_{22}^{\mathrm{INT}} + R_s) Y_{jd}] + R_d \quad , \quad (7)$$

with

$$Y_{jd} = j\omega C_{jd} / (1 + j\omega R_{sub} C_{jd}) \quad , \quad (8)$$

$$N = Z_{11}^{\mathrm{INT}} Z_{22}^{\mathrm{INT}} - Z_{12}^{\mathrm{INT}} Z_{21}^{\mathrm{INT}} + R_s (Z_{11}^{\mathrm{INT}} + Z_{22}^{\mathrm{INT}} - Z_{12}^{\mathrm{INT}} - Z_{21}^{\mathrm{INT}}) \quad . \quad (9)$$

Z_{pq}^{INT} can be converted into the Y-parameters Y_{pq}^{INT}, the values of intrinsic elements can be determined using Eqs. 10-15:

$$R_{ds} = 1 / \mathrm{Re}(Y_{22}^{\mathrm{INT}}) \quad , \quad (10)$$

$$C_{ds} = [\mathrm{Im}(Y_{12}^{\mathrm{INT}}) + \mathrm{Im}(Y_{22}^{\mathrm{INT}})] / \omega \quad , \quad (11)$$

$$C_{ds} = [\mathrm{Im}(Y_{11}^{\mathrm{INT}}) + \mathrm{Im}(Y_{12}^{\mathrm{INT}})] / \omega \quad , \quad (12)$$

$$C_{gd} = \mathrm{Im}(Y_{12}^{\mathrm{INT}}) / \omega \quad , \quad (13)$$

$$\tau = \arctan[\mathrm{Im}(Y_{21}^{\mathrm{INT}} - Y_{12}^{\mathrm{INT}})] / \omega \mathrm{Re}(Y_{21}^{\mathrm{INT}} - Y_{12}^{\mathrm{INT}}) \quad , \quad (14)$$

$$g_m = \mathrm{Re}(Y_{21}^{\mathrm{INT}}) / \cos(\omega\tau) \quad , \quad (15)$$

where ω is the angular frequency.

The values of R_g, R_d, R_s, C_{jd} and R_{sub} are updated to reduce the discrepancy of the simulated S-parameters and the measured S-parameters ε. ε is set as the optimization criterion. Based on the semi-analytical method, all the elements can be extracted.

$$\varepsilon = \sum_{p=1}^{2} \sum_{q=1}^{2} \sum_{i=0}^{N\ 1} W_{pq} | S_{pq}^{S}(\omega_i, R_g, R_s, R_d, C_{jd}, R_{sub}) \quad S_{pq}^{M}(\omega_i, R_g, R_s, R_d, C_{jd}, R_{sub}) | \quad . \quad (16)$$

Superscript S denotes the simulated S-parameters, and M represents the measured S-parameters.

Step 2

After all the parameters of the one cell in the conventional way (shown in Fig. 5) are extracted, using the parameters, the values of the elements inside elementary cells can be determined by Eqs. 17-20. The elementary cells are in parallel with each other. As is shown in Eq. 17, the gatewidth of the conventional one cell equals the total gatewidth of all elementary cells. According to previous investigation in Ref. [2], the extrinsic resistances of elementary cell R_g, R_d, R_s and series bulk resistance R_{sub} are inversely proportional to device gatewidth, and the drain-to-bulk capacitance C_{jd} is proportional to the gatewidth of the elementary cell. For the intrinsic part, the capacitances C_{gs}, C_{gd}, C_{ds} and transconductance g_m are proportional to device gatewidth, the channel resistance R_{ds} is inversely proportional to the device gatewidth.

$$W^e = W / n \quad , \quad (17)$$

$$R_{(g,d,s,ds,sub)}^{e} = n R_{(g,d,s,ds,sub)} \quad , \quad (18)$$

$$C_{(gs,gd,ds,jd)}^{e} = C_{(gs,gd,ds,jd)} / n \quad , \quad (19)$$

$$g_m^e = g_m / n \quad , \quad (20)$$

where n is the number of the elementary cells. The parameters with superscript e are for the elementary cells.

Step 3

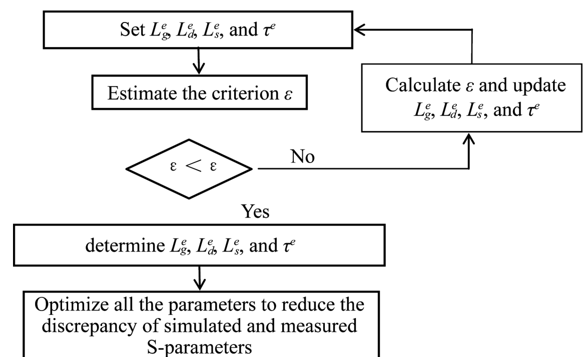

Fig. 6 The flowchart of extracting parameters
图 6 参数提取过程的流程图

All the parameters can be obtained except L_g^e, L_d^e, L_s^e and τ^e. In the optimization procedure, L_g^e, L_d^e, L_s^e and

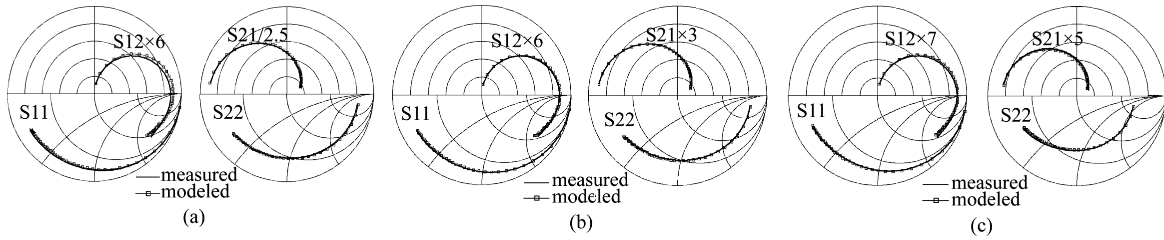

Fig. 7　Comparison of measured and modeled S-parameters for the MOSFET in the frequency range of 1 ~ 40 GHz, (a) V_{gs} = 0.6 V and V_{ds} = 0.6 V, (b) V_{gs} = 0.6 V and V_{ds} = 1.0 V, (c) V_{gs} = 0.8 V and V_{ds} = 0.8 V
图 7　1 ~ 40 GHz 范围内 MOSFET 器件的测量 S 参数和改进模型仿真 S 参数的对比，(a) V_{gs} = 0.6 V and V_{ds} = 0.6 V, (b) V_{gs} = 0.6 V and V_{ds} = 1.0 V, (c) V_{gs} = 0.8 V and V_{ds} = 0.8 V

τ^e are set as independent variables, the discrepancy of the simulated S-parameters and the measured S-parameters ε (calculated as equation 16) is set as the optimization criterion. L_g^e, L_d^e, L_s^e and τ^e are updated to reduce ε. The flowchart to determine all the parameters is shown in Fig. 7.

3　Results and Discussion

In order to verify the above method, the proposed equivalent circuit model shown in Fig. 4 is implemented to simulate the device in Advanced Design System (ADS), the device is 90-nm NMOSFET transistor with 8 × 0.6 × 12 μm (number of gate fingers unit gatewidth cells). The Infineon Technologies 90-nm CMOS technology is a stable and high-yield technology with low variation between wafers or different lots. The measurement for extraction and verification was performed in the frequency range of 1-40 G using an Agilent 8510C network analyzer. DC bias was supplied by an Agilent 4 156 A.

Table 1　The parasitic elements of the test structure
表 1　测试结构的寄生参数

Parameters	Values	Units	Parameters	Values	Units
C_{pg}	121	fF	R_{ldb}	3	Ω
C_{pd}	117	fF	R_{lsb}	6.5	Ω
C_{pgd}	1.2	fF	L_{lga}	30	pH
R_{pg}	9.8	Ω	L_{lda}	31	pH
R_{pd}	10.5	Ω	L_{lsa}	0.1	pH
R_{lga}	0.4	Ω	L_{lgb}	10	pH
R_{lda}	0.34	Ω	L_{ldb}	10	pH
R_{lsa}	0.18	Ω	L_{lsb}	5.5	pH
R_{lgb}	3	Ω			

Table 2　The elements of the elementary cells in the proposed model
表 2　改进模型中元胞内部的元件参数

Parameters	Values	Units	Parameters	Values	Units
R_g	12	Ω	R_{ds}	6 000	Ω
R_s	10	Ω	C_{ds}	1.5	fF
R_d	20	Ω	C_{gd}	2.8	fF
C_{jd}	1.5	fF	C_{gs}	5.5	fF
R_{sub}	1 400	Ω	τ	0.3	ps
g_m	2.1	mS	L_d	140	pH
L_g	200	pH	L_s	60	pH

The parasitic elements of the test structure are listed in Table I. Table II summarizes the extracted parameters of the proposed model using the method above. The parameters obtained are physically meaningful, which is validated by the agreement of the simulated and measured results.

The simulated result is confronted with measured data in Fig. 7, notice that a good model-experimental correlation is observed. This verifies the validity of the extractions performed above.

To demonstrate the improvement over the conventional models, the comparison of accuracy between three models is displayed in Fig. 8. It can be clearly found that the accuracy (relative error) of the proposed model (C line) is better than the two conventional models (A line and B line), especially in high frequency range. The proposed model incorporates the skin effect of feedlines and multiple cells. Two conventional models are the one - cell model considering skin effect and the multiple -

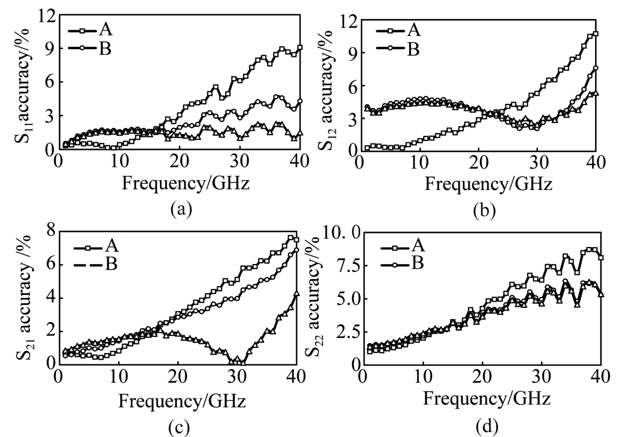

Fig. 8　Comparison of accuracy between proposed and conventional models in the frequency range of 1 ~ 40 GHz at the bias of V_{gs} = 0.6 V and V_{ds} = 0.6 V. Curve: (A) accuracy of S-parameters of one-cell model with skin effect, Curve: (B) accuracy of S-parameters of multiple-cell model without skin effect, Curve: (C) accuracy of S-parameters of multiple-cell model with skin effect
图 8　1 ~ 40 GHz 范围内改进模型与传统模型的精度对比，偏置电压为：V_{gs} = 0.6 V，V_{ds} = 0.6 V，曲线(A)考虑趋肤效应的单胞模型精度，曲线(B)未考虑趋肤效应的多胞模型精度，曲线(C)考虑趋肤效应的多胞模型精度

(下转第 562 页)

impedance of porous electrodes[J]. *Electrochimica Acta*, 2015, 160: 313-322.

[2]WANG Bo, WU Gong-ping, XU Chang-ming, *et al*. Research and development of backstage management and inspection system based on transmission line inspection robot[J]. *Engineering Journal of Wuhan University*(王波,吴功平,许昌明,等. 输电线路巡检机器人后台管理及诊断系统. **武汉大学学报**: 工学版), 2014, **47**(1): 110-114.

[3]ZHAO Yu, WANG Xian-pei, HU Hong-hong, *et al*. Early Warning for Various Internet Faults of GIS Based on Ultraviolet Spectroscopy [J]. *Spectroscopy and Spectral*(赵宇,王先陪,胡红红,等. 基于紫外光谱检测的GIS内多类故障早期预警,**光谱学与光谱分析**), 2015:02-15.

[4]FANG Ting, DONG Chong, HU Xing-liu, *et al*. Contour Extraction and Fault Detection of Insulator Strings in Aerial Images[J]. *Journal of shanghai jiaotong university*(方挺,董冲,胡兴柳,等. 航拍图像中绝缘子串的轮廓提取和故障检测. **上海交通大学学报**),2013(12).

[5]GE Yu-min, LI Bao-shu, ZHAO Shu-tao, *et al*. A method based on aerial images to detect the surface state of insulators[J]. *High Voltage Apparatus*(葛玉敏,李宝树,赵书涛,等. 基于航拍图像的绝缘子表面状态检测. **高压电器**), 2010(04).

[6]Kyrchanova O, Mogila V, Wolle D, *et al*. Functional Dissection of the Blocking and Bypass Activities of the Fab-8 Boundary in the Drosophila Bithorax Complex[J]. *PLoS Genet*, 2016, **12**(7): e1006188.

[7]GE Yu-min, LI Bao-shu, LIANG Shuang. A method based on aerial images to detect the surface state of insulators[J]. High Voltage Apparatus(葛玉敏,李宝树,梁爽. 数学形态学在绝缘子图像边缘检测中的应用. **高压电器**), 2012, **48**(1): 101-104.

[8]FANG Ting, DONG Chong, HU Xing-liu, *et al*. Counter extraction and fault detection of insulator strings in aerial images[J]. *Journal of Shanghai Jiaotong university*(方挺,董冲,胡兴柳,等. 航拍图像中绝缘子串的轮廓提取和故障检测. **上海交通大学学报**), 2013, **47**(012): 1818-1822.

[9]Saranya K, Muniraj C. A SVM Based Condition Monitoring of Transmission Line Insulators Using PMU for Smart Grid Environment[J]. *Journal of Power and Energy Engineering*, 2016, **4**(03): 47.

[10]Zhai Y, Wang D, Zhang M, *et al*. Fault detection of insulator based on saliency and adaptive morphology[J]. *Multimedia Tools and Applications*, 2016: 1-14.

[11]WU Yi-nan, LI Guo-ning, ZHANG Ning. Calculation of overlapping pixels in interleaving assembly for CCD focal plane of space camera [J]. *Optics and Precision Engineering*(武奕楠,李国宁,张宇. 空间相机焦平面CCD交错拼接重叠像元数计算. **光学精密工程**), 2016, **24**(2): 422-429.

[12]Kyrchanova O V, Leman D V, Toshchakov S V, *et al*. Induction of transcription through the scs insulator leads to abnormal development of Drosophila melanogaster[J]. *Russian Journal of Genetics*, 2016, **52**(10):1007-1014.

[13]Kyrchanova O, Mogila V, Wolle D, *et al*. Functional Dissection of the Blocking and Bypass Activities of the Fab-8 Boundary in the Drosophila Bithorax Complex[J]. *PLoS Genet*, 2016, **12**(7): e1006188.

[14]Avva S V S P. Characterization of Boundary Element-Associated Factors BEAF-32A and BEAF-32B and Identification of Novel Interaction Partners in Drosophila Melanogaster[D]. Faculty of the Louisiana State University and Agricultural and Mechanical College in partial fulfillment of the requirements for the degree of Doctor of Philosophy in The Department of Biological Sciences by SV Satya Prakash Avva B. Tech., ICFAI University, 2016.

[15]Sadeghi L. Modulating chromatin by transcription and nucleosome turnover: a genome-wide study in fission yeast [M]. Inst förbiovetenskaperochn ringsl ra/Dept of Biosciences and Nutrition, 2015.

[16]Sadeghi L. Modulating chromatin by transcription and nucleosome turnover: a genome-wide study in fission yeast[J]. 2015.

[17]Griffin D K, Fowler K E, Peter J, *et al*. 20th International Chromosome Conference (ICCXX)[J]. *Chromosome Research*, 2015, **23**(2): 343.

[18]Sunagar K, Jackson T N W, Undheim E A B, *et al*. Three-fingered RAVERs: rapid accumulation of variations in exposed residues of snake venom toxins[J]. *Toxins*, 2013, **5**(11): 2172-2208.

[19]Wu Y, Wang Y, Jia Y. Segmentation of the left ventricle in cardiac cine MRI using a shape-constrained snake model[J]. *Computer Vision and Image Understanding*, 2013, **117**(9):990-1003.

[20]WANG Le-yang, XU Cai-jun. Voxels and the construction of a virtual geographic environment[J]. *Geomatics and information science of Wuhan univetsity*(王乐洋,许才军. 总体最小二乘研究进展 **武汉大学学报**: 信息科学版), 2013, **38**(7): 850-856.

(上接第553页)

cell model without skin effect. The deviation is 2% for S_{11}, 3% for S_{12}, 1.5% for S_{21} and 4% for S_{22}.

4 Conclusion

An improved small-signal model for nanometer MOSFET device is developed in this paper. The better result is achieved by modeling the MOSFET with multiple cells considering skin effect of feedlines. It is more desirable to take the effect of interconnection between elementary cells into account. According to the parameters of the conventional one cell model, physically expected results are obtained for the parameters of multiple cells. The validity of the new model is proven by comparison with measured S-parameters up to 40 GHz.

References

[1]Allam E A, Manku T. A small-signal MOSFET model for radio frequency IC applications [J]. *IEEE Transactions on Computer-Aided Design of Integrated Circuits and Systems*. 1997, **16**(5):437-447.

[2]GAO Jian-Jun, Werthof A. Direct parameter extraction method for deep submicrometer metal oxide semiconductor field effect transistor small signal equivalent circuit [J]. *IET Microwave, Antennas and Propagation*. 2009, **3**(4):564-571.

[3]Xu Jian-Fei, Yan Nan, Zeng X, Gao Jian-Jun. A 3.4 dB NF k-band LNA with a tapped capacitor matching network in 65 nm CMOS technology [J]. *International Journal of RF and Microwave Computer-Aided Engineering*. 2015, **25**(2):146-153.

[4]Eo Y, Eisenstadt W R. High-speed VLSI interconnect modeling based on S-parameter measurements [J]. *IEEE Transaction On Components, Hybrids, and Manufacturing Technology*. 1993, **16**(5):555-562.

[5]Kwon I, Je M, Lee K, *et al*. A simple and analytical parameter-extraction method of a microwave MOSFET [J]. *IEEE Transactions on Microwave Theory and Techniques*. 2002, **50**(6):1503-1509.

[6]Mei S, Ismail Y I. Modeling skin and proximity effects with reduced realizable RL circuits [J]. *IEEE Transaction on Very Large Scale Integration System*. 2004, **12**(4):437-447.

[7]Gao Jian-Jun, Werthof A. Scalable small-signal and noise modeling for deep-submicrometer MOSFETs [J]. *IEEE Transactions on Microwave Theory and Techniques*. 2009, **57**(4):737-744.